THE JOURNAL OF PHYSICAL CHEMISTRY A

Article

pubs.acs.org/JPCA

Structural Differentiation between Layered Single (Ni) and Double Metal Hydroxides (Ni–Al LDHs) Using Wavelet Transformation

Matthew G. Siebecker*,† and Donald L. Sparks†

†University of Delaware, Delaware Environmental Institute (DENIN), Interdisciplinary Science and Engineering (ISE) Laboratory, 221 Academy Street, Newark, Delaware 19716, United States

Supporting Information

ABSTRACT: Layered double hydroxides (LDHs) are anionic clays important in disciplines such as environmental chemistry, geochemistry, and materials science. Developments in signal processing of extended X-ray absorption fine structure (EXAFS) data, such as wavelet transformation (WT), have been used to identify transition metals and Al present in the hydroxide sheets of LDHs. The WT plots of LDHs should be distinct from those of isostructural single metal hydroxides. However, no direct comparison of these minerals appears in the literature using WT. This work systematically analyzes a suite of Ni-rich mineral standards, including Ni–Al LDHs, single metal Ni hydroxides, and Ni-rich silicates using WT. The results illustrate that the WT plots for α-Ni(OH)$_2$ and Ni–Al LDHs are often indistinguishable from each other, with similar two-component plots for the different mineral types. This demonstrates that the WT of the first metal shell often cannot be used to differentiate an LDH from a single metal hydroxide. Interlayer anions adsorbed to the hydroxide sheet of α-Ni(OH)$_2$ affect the EXAFS spectra and are not visible in the FT but are clearly resolved and discrete in the WT.

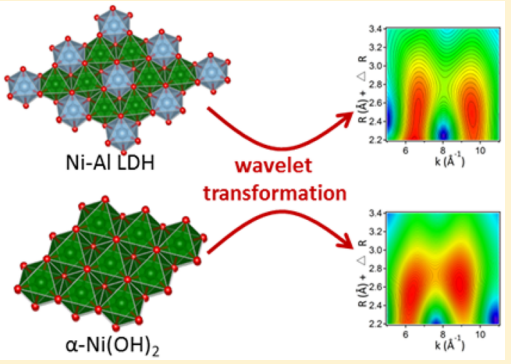

1. INTRODUCTION

Layered double hydroxides (LDHs) are a class of anionic clays important to research areas such as environmental chemistry, geochemistry, materials science, and catalysis.[1−5] In environmental geochemical systems, such as in soils and sediments, LDHs rich in aluminum (Al) are important in the cycling and precipitation of trace metal contaminants. Nickel (Ni) in particular can form Ni–Al LDHs to potentially inhibit Ni mobility.[6−9] Other transition metals can form LDHs with Al in geochemical systems, including zinc (Zn), ferrous iron (Fe^{2+}), and cobalt (Co).[10−14]

The formation of Ni–Al LDH is important because LDHs have lower solubility product constants than the single metal hydroxides [e.g., α-Ni(OH)$_2$].[3,4] Thus, the LDH can control the solution concentrations of the trace metal. However, LDHs are isostructural to single metal hydroxides, and thus differentiating between the two mineral types is difficult. Extended X-ray absorption fine structure (EXAFS) spectroscopy has been one tool used to identify the molecular structure of Ni–Al LDHs and is also used to characterize single metal hydroxides.[15,16] However, traditional analysis of EXAFS data [e.g., shell fitting of the Fourier transform (FT)] is particularly challenging because of the structural similarities between Ni–Al LDHs and single metal Ni hydroxides.[5] The in-and-out-of-phase backscattering photoelectric waves of elements such as Ni, Al, and Si create constructive and destructive interference in the EXAFS data, making shell fitting difficult.[17]

Developments in signal processing of EXAFS data, such as wavelet transformation (WT), have made differentiation between Ni and Al backscatters more straightforward.[18] However, there are no comparative studies that apply WT to single metal hydroxides as well. WT is capable of separating the contribution of Ni from Al backscattering in the hydroxide sheet of the LDH into two discrete components. WT resolves the data in both k-and r-space simultaneously[18] to identify if more than one type of backscatterer (either from an atom or multiple scattering) is contributing to the EXAFS data. It is particularly useful for separating elements of significantly different atomic weights, such as transition metals (e.g., Ni, Fe, Zn) from Al. It is becoming commonly applied to EXAFS spectra to identify and characterize not only LDHs in geochemical systems but also other chemical environments such as C and Fe.[6,7,9,18−23]

The objective of this work was to systematically analyze and compare a suite of Ni-rich mineral standards, including Ni–Al LDHs, single metal Ni hydroxides [e.g., α-Ni(OH)$_2$ and β-Ni(OH)$_2$], and Ni-rich silicates (e.g., silicated Ni–Al LDHs and Ni-phyllosilicates). Because WT is becoming a frequent tool in the analysis of X-ray absorption spectroscopic (XAS) data, there is a need for comparative data in the literature to illustrate its use. Comparison and analysis presented here illustrate the

Received: August 9, 2017
Revised: August 19, 2017
Published: August 23, 2017

DOI: 10.1021/acs.jpca.7b07940
J. Phys. Chem. A XXXX, XXX, XXX−XXX

effects of modifying the adjustable parameters of the WT (η and σ), and how appropriate conclusions can be made on the number and type of backscattering components in EXAFS spectra. Because the solubility of LDHs, single metal hydroxides, and silicates vary considerably, accurate identification of these minerals is necessary in environmental geochemical systems.

2. EXPERIMENTAL METHODS

2.1. EXAFS Data. Table 1 lists the 24 Ni-rich mineral standards analyzed by WT. References for previously published spectra are given in Table 1 along with the Ni-to-Al ratios in the LDHs. Previously unpublished spectra are indicated and shell fitting results of those spectra are given in the Supporting Information (SI) Table S1. Shell fitting was carried out with Artemis software.[24] EXAFS spectra of the 24 standards along with their FT are in Figure 1.

Table 1. Spectra of Layered Ni-Rich Minerals (24 Total) Analyzed by WT[a]

sample	ref
α-Ni(OH)$_2$ #1	this work
α-Ni(OH)$_2$ #2	16
α-Ni(OH)$_2$ #3	this work
α-Ni(OH)$_2$ #4	this work
β-Ni(OH)$_2$ #5	16
α-Ni(OH)$_2$ #6	CARS
α-Ni(OH)$_2$ #7	this work
α-Ni(OH)$_2$ #8	this work
α-Ni(OH)$_2$ #9	33
β-Ni(OH)$_2$ #10	33
α-Ni(OH)$_2$ #11	15
β-Ni(OH)$_2$ #12	15
Ni basic nitrate	33
LDH #1 (Ni:Al ratio = 1.78:1)	4
LDH #2 (Ni:Al ratio = 1.3:1)	16
LDH #3 (Ni:Al ratio = 4.3:1)	16
LDH #4 (Ni:Al ratio = 1.94:1, aged 65 °C)	4
LDH #5 (Ni:Al ratio = 5.49:1)	This work
LDH #6 (Ni:Al ratio = 2:1)	33
LDH silicate #1 (Ni:Al ratio = 1.86:1)	4
LDH silicate #2 (Ni:Al ratio = 2.3:1)	26
Ni silicate #1	26
Ni silicate #2	4
LDH-py	9

[a]Spectra from the literature are accompanied by their references. Structural fitting results for the spectra presented in this work are in Table S1. Structural models for Ni-rich minerals can be found in Figure S6. Only samples prepared explicitly as β-Ni(OH)$_2$ are labeled as such. Ni-to-Al ratios are given for each LDH.

With respect to the published Ni(OH)$_2$ spectra, original data for α-Ni(OH)$_2$ #2 and β-Ni(OH)$_2$ #5 were used from ref 16. The α-Ni(OH)$_2$ #6 spectrum was obtained from an online EXAFS data library hosted by the University of Chicago Center for Advanced Radiation Sources (CARS). Spectra from ref 33 (including the Ni basic nitrate) and ref 15 were digitized[25] from the published manuscripts and rebinned at 0.05 Å^{-1} in k-space with Origin 2017 graphing software. These spectra included α-Ni(OH)$_2$ #9, β-Ni(OH)$_2$ #10, α-Ni(OH)$_2$ #11, β-Ni(OH)$_2$ #12, and Ni basic nitrate. To facilitate sample identification, α- and β-Ni(OH)$_2$ spectra were grouped into the same consecutive numeric sequence.

In addition to published single metal Ni hydroxides, published LDH spectra were also used, including original data from refs 4 and16 (LDH #1 to LDH #4). LDH #1 and LDH #4 were synthesized with 1.78:1 and 1.94:1 Ni:Al ratios, respectively, and have a carbonate interlayer, while LDH #4 was additionally aged for 2 weeks at 65 °C. LDH #2 and #3 have Ni:Al ratios of 1.3 and 4.3, respectively.[16] LDH #6 from ref 33 was digitized and rebinned as stated and has a Ni:Al ratio of 2. Original data for Ni−Al LDH silicates #1 and #2, Ni silicates #1 and #2, and Ni reacted with pyrophyllite for five years ("LDH-py") were used, and all have silicate incorporated into the interlayer space.[4,9,26]

Published and previously characterized EXAFS spectra compose a significant portion of data used here for WT and provide a key basis for comparison between LDH and Ni(OH)$_2$ phases. In addition to the previously published spectra, new unpublished spectra (this work, Table 1) are also presented and analyzed by WT. Shell fitting results characterizing those spectra are in Supporting Information, Table S1. α-Ni(OH)$_2$ #1 was purchase from Johnson Matthey company, and data were collected at the National Synchrotron Light Source (NSLS) beamline X-18B under QXAS scanning mode.[27] The remaining α-Ni(OH)$_2$ standards (#3, #4, #7, and #8) were synthesized according to published methods,[16,28] and EXAFS spectra were collected at the NSLS beamline X-11A. LDH #5 was synthesized according to ref 29, and EXAFS spectra were collected at NSLS beamline X-11-A as well. All LDH spectra are Ni−Al LDHs. All fitting and WT was carried out with a k-weight of 3.

2.2. Wavelet Transformation. WT was carried out with the HAMA program written for IGORpro.[18,30] In the WT expression, two adjustable parameters [eta (η) and sigma (σ)] are used to focus on an overview WT or detailed WT. For the overview WT, $\eta\cdot\sigma \geq 30$, and for the detailed WT, $\eta\cdot\sigma \approx 2r$, where r is the distance of interest in R-space. For WT of the first metal shell (Figures 2 and 3, and Figures S1 and S2), the product of the eta (η) and sigma (σ) values were adjusted for optimal resolution in both k and r space, which is twice the distance of interest in r-space ($\eta\cdot\sigma \approx 2r$).[31] Specifically, η = 30 and σ = 0.18 ($\eta\cdot\sigma$ = 5.4) whose product is similar to other values in the literature.[18,20,32] For the third metal shell (Figures 2 and Figures S3 and S4) it was determined that values η = 30 and σ = 0.17 provided the necessary resolution to separate Ni and Al. A series of values for η and σ were tested for the second and third metal shells (Figure S5) to determine optimal parameter values. R-ranges for WT varied depending on the shell of interest, and the precise values are located on the y-axis of each WT plot. WT was carried out on the k ranges of the data presented in Figure 1, except for LDH #6, α-Ni(OH)$_2$ #9, and β-Ni(OH)$_2$ #10, where a k-range 3 to 15 Å^{-1} was used.

3. RESULTS AND DISCUSSION

WT facilitates differentiation between heavier and lighter backscattering elements (e.g., Ni and Al) when they are at the same distance (i.e., the same coordination shell) from the central absorbing atom. It provides a visualization of the r and k dependencies of neighboring atoms and resolves the EXAFS spectra in both r and k spaces. WT is analogous to the FT, but the data are spread over an x−y plane in two dimensions. This type of discrimination is not possible if only using the FT. While the FT resolves the distances of the backscattering

DOI: 10.1021/acs.jpca.7b07940
J. Phys. Chem. A XXXX, XXX, XXX−XXX

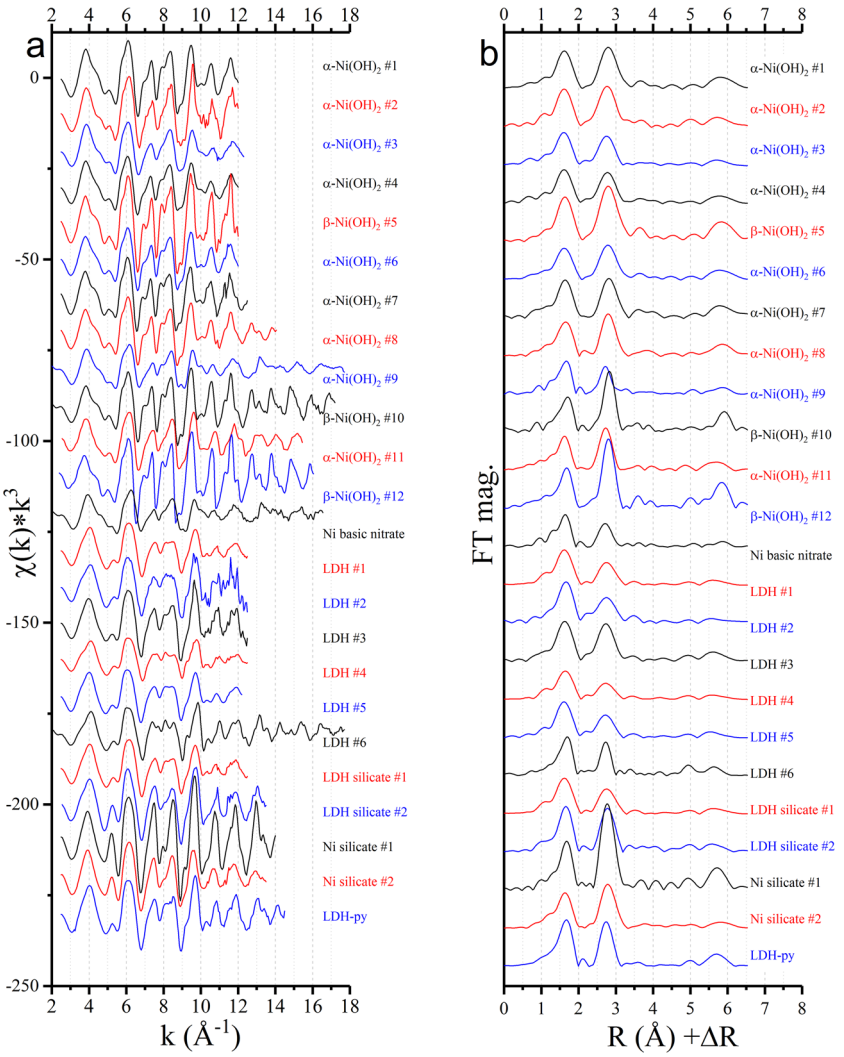

Figure 1. (a) EXAFS spectra of the 24 Ni-rich mineral, and (b) the FT of those spectra. Each spectrum label corresponds to Table 1. The major differences in the EXAFS spectra between α- and β-phase $Ni(OH)_2$ are the increased doublet peaks at ca. 7 $Å^{-1}$ and 8 $Å^{-1}$. β-$Ni(OH)_2$ #5, #10, and #12 exhibit these doublet peaks more than other $Ni(OH)_2$ spectra.

atoms, WT reveals additionally at which energies (wavenumbers, in $Å^{-1}$) the backscattering components are most significant.[18,20,22]

This transformation process is particularly useful for the Ni–Al LDH system because both heavy (Ni) and light (Al) atoms are in its hydroxide sheet and first metal coordination shell around Ni. Two distinct regions in the WT plot represent the different types of atomic backscattering contributions present in the EXAFS data. Lighter and heavier elements at the same distance around the central absorbing Ni atom cause interference between several distinct backscattering waves, which significantly complicates EXAFS modeling.[20] The second and third metal shells also provide useful information in the WT. In LDHs, those peaks result from the focused multiple scattering of Ni and Al in the hydroxide sheet (Figure S7).[16,20,34] The presence of light and heavy backscatterers is indicated in the WT plots by the separate maxima at different wavenumbers.

3.1. Ideal WT Plots: LDHs vs $Ni(OH)_2$. Figure 2 contains the WT plots of samples LDH #4 and α-$Ni(OH)_2$ #2. These plots represent the ideal number of components in the first and third metal shells of a layered single and double metal hydroxide. The first metal shell of the LDH contains both Ni and Al (Figure S7), and the two components seen in Figure 2a can be ascribed to these two atoms.[18] One component at lower energy between 6 and 7 $Å^{-1}$ and the other component at higher energy between 9 and 10 $Å^{-1}$ can be attributed to Al and Ni, respectively.[6,9,18] Figure 2a is directly comparable to Figure 2c, which is the WT of α-$Ni(OH)_2$ #2. Because the hydroxide sheet of the single metal Ni hydroxide has one metal atom type, there is one major component in red at ca. 9 $Å^{-1}$. However, there is a minor component between 6 and 7 $Å^{-1}$ that appears as a less intense component in orange, and it is hypothesized that this minor component can be attributed to anion sorption (such as nitrate) to the hydroxide sheet. This sample, α-$Ni(OH)_2$ #2 from ref 16, has some nitrato groups covalently bonded to the hydroxide sheet as indicated in its IR spectrum. Of all the α-$Ni(OH)_2$ spectra presented (Figure S2) the WT plot of α-$Ni(OH)_2$ #2 has the smallest secondary component between 6 and 7 $Å^{-1}$. All the other WT plots of α-$Ni(OH)_2$ have more significant secondary components and are indistinguishable from the WT plots of LDHs (Figure S1).

Figure 2 panels b and d are also directly comparable and are WT plots of the third metal shells of the same samples. In the third metal shell, again there should be two atom types in the LDH[20] and one atom type in the single metal hydroxide (see

DOI: 10.1021/acs.jpca.7b07940
J. Phys. Chem. A XXXX, XXX, XXX−XXX

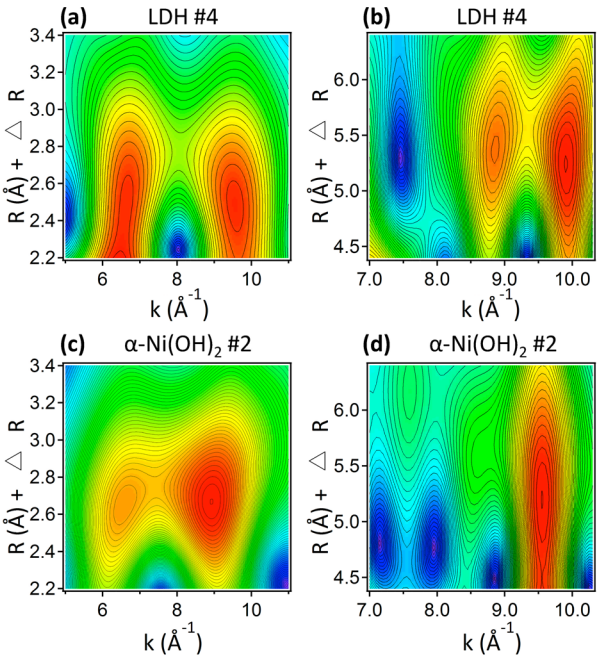

Figure 2. WT plots of the (a) first and (b) third metal shells of LDH #4, and WT plots of the (c) first and (d) third metal shells of α-$Ni(OH)_2$ #2. The red areas indicate where significant components are separated in the WT. The LDH has two components in both its first and third metal shells, which is expected from the ideal structural model (Figure S7). The WT of α-$Ni(OH)_2$ #2 indicates in the first shell one major component is present (red) while a second minor component is also present (orange). The third metal shell of α-$Ni(OH)_2$ #2 has just one component (red). These ideal WT plots do not consistently occur for the first and third metal shells (Figures S1–S4).

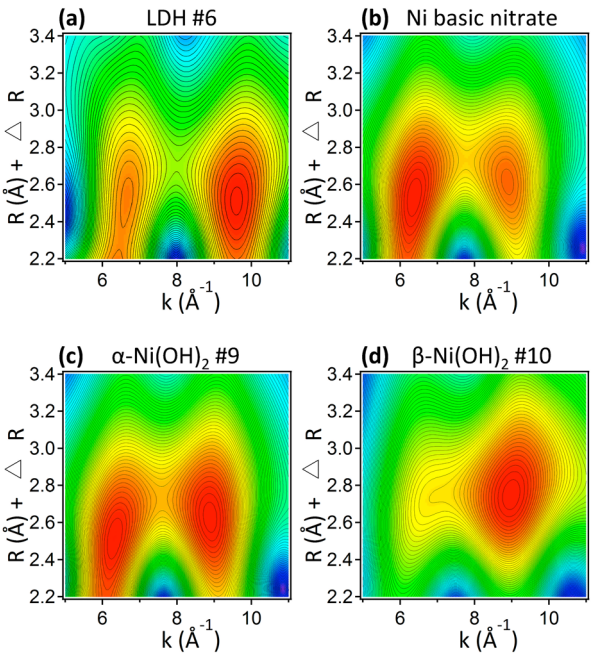

Figure 3. First metal shell WT plots of four EXAFS spectra from ref 33. (a) LDH #6 (Ni–Al LDH 2:1 Ni:Al ratio), (b) Ni basic nitrate, (c) α-$Ni(OH)_2$ #9, and (d) β-$Ni(OH)_2$ #10. The plot of LDH #6 is as expected, with two major components (one at low and one at high energy, $Å^{-1}$). The Ni basic nitrate illustrates how a similar WT plot can be generated without the presence of Al in the sample. α-$Ni(OH)_2$ #9 also has no Al but produces a similar WT to both the LDH and Ni basic nitrate. Of the four plots, that of β-$Ni(OH)_2$ #10 is the only spectrum to present a WT displaying just one component.

Figure S6 for mineral structural models). Figure 2 panels b and d represent the ideal WT plots of what the LDHs and single metal hydroxides should look like. The LDH has two components in the WT plot, one component at lower energy between 8.5 and 9.5 $Å^{-1}$ and the other component at higher energy between 9.5 and 10.3 $Å^{-1}$. The single metal Ni hydroxide has just one major component (between 9 and 10 $Å^{-1}$) because it has just one atom type in its hydroxide sheet (Figure S6). As discussed in sections 3.3 and 3.4, these ideal WT plots do not consistently occur even in the third metal shell. Thus, for environmental geochemical samples, the use of WT for distinction between the LDH and single metal hydroxides is limited.

3.2. Effect of Interlayer Anion. To test the hypothesis that covalently bonded interlayer anions could be identified in the WT plots, WT was carried out on a series of four EXAFS standards from ref 33 (Figure 3). The standards from that work included "NiAl2", "Ni basic nitrate", "α-$Ni(OH)_2$", and "β-$Ni(OH)_2$", which are labeled here as LDH #6, Ni basic nitrate, α-$Ni(OH)_2$ #9, and β-$Ni(OH)_2$ #10, respectively. The standard LDH #6 is a Ni–Al LDH with a Ni:Al ratio of 2:1. The WT plot of LDH #6 yields the predicted result with two major components contributing to the EXAFS spectrum, one component at lower energy between 6 and 7 $Å^{-1}$ and the other component at higher energy between 9 and 10 $Å^{-1}$ (Figure 3a). The first component at lower energy can be attributed to Al scattering and the second component at higher energy to Ni scattering. The plot of Ni basic nitrate (Figure 3b) illustrates the effect of covalently bonded nitrato groups on the WT. This sample was deliberately synthesized to contain nitrato groups in its structure, covalently bonded to the hydroxide sheet.[33]

As hypothesized, when WT was carried out on the Ni basic nitrate EXAFS spectrum, two components are also present, making the WT plot indistinguishable from the LDH plot. This occurs even though the hydroxide sheet of the Ni basic nitrate only contains one type of metal atom (Ni). The Ni basic nitrate is analogous to the α-$Ni(OH)_2$ structure except that some of the OH groups are replaced by NO_3 groups. The infrared (IR) spectra from this sample clearly indicate and describe the presence of both nitrate in the interlayer and nitrato groups covalently bonded in the hydroxide sheet (see ref 33).

The interlayer anion can thus have an effect on the first metal shell radial structure function (RSF) which is not apparent in the FT but clearly discernible in the WT plot. In addition to the Ni basic nitrate spectrum, the IR spectrum for α-$Ni(OH)_2$ #9 also indicates some adsorption of nitrato groups. The WT plot for α-$Ni(OH)_2$ #9 (Figure 3c) indicates the presence of two components in the first metal shell even though the hydroxide sheet still contains only Ni atoms (Figure S6). The WT plot of α-$Ni(OH)_2$ #9 is also indistinguishable from the LDH because both plots have two components, one at low and one at high energy. Figure 3 panels a–c are very similar to each other but the samples have different chemical compositions.

The data set in Figure 3, the EXAFS and related IR spectra of which were originally published by ref 33, serves to illustrate how different forms of structurally similar yet chemically distinct minerals can produce similar WT plots. LDH #6, Ni basic nitrate, and α-$Ni(OH)_2$ #9 all contain two components in their WT plots. The only compound with no nitrato groups or

DOI: 10.1021/acs.jpca.7b07940
J. Phys. Chem. A XXXX, XXX, XXX–XXX

nitrate in its IR spectrum (and thus absent from the interlayer) is β-Ni(OH)$_2$ #9 (Figure 3d). This difference is also clear in the WT plot because only one component is present. The increase in crystallinity and decrease in the *c*-axis probably cause the absence of interlayer anions. Other β-Ni(OH)$_2$ phases presented (which include β-Ni(OH)$_2$ #5 and β-Ni(OH)$_2$ #12) also yield WT plots with just one major component (Figure S2). This finding is reproducible across three different samples from the literature.

3.3. First Metal Shell Similarities. The main advantage of using WT is that it can separate multiple components in a single coordination shell. Thus, it was hypothesized that the first metal shell of the six LDHs presented would include two significant components, as has been demonstrated in the literature.[18] Indeed, the first metal shell of all six LDHs contains two components (Figure S1).

However, the other spectra in Figure S1 also contain, in general, two components. These minerals include two silicated LDHs, two Ni silicates, one adsorption sample of Ni to pyrophyllite, and one Ni basic nitrate (for comparison). As indicated in Figure S6, the chemical differences between the samples include multiple elements in the first metal shell and for the silicates a separate tetrahedral layer of Si. In all of these samples, it would be predicted that there are two components in the first metal shell because the silicates include Si at approximately 3.22−3.29 Å.[16,35] The spectrum for Ni sorbed to pyrophyllite has been discussed as forming an LDH,[9] and so the presence of two components is expected.

Because the standards in Figure S1 are confirmed to have two components in the first metal shell, resulting from the presence of Al, Si, or covalently bonded nitrato groups, it was hypothesized that the first metal shell for all Ni(OH)$_2$ standards [Ni(OH)$_2$ #1−#12, Table 1, Figure 1, and Figure S2] should contain just one major component. This should be the case because there is only one metal type (Ni) in the hydroxide sheet (Figure S6). However, as shown in Figure S2, most of the Ni(OH)$_2$ phases also contain two major components in the WT plots. The presence of two components where ideally there should be just one component is probably due to the presence of adsorbed anions to the hydroxide sheet, as shown in Figure 3b. The similarity between the data in Figures S1 and S2 make it difficult to use WT alone to confirm the presence or absence of Al in the Ni−Al LDH.

Alluded to in section 3.1, the lack of differences in the WT plots of LDHs and single metal hydroxides can be a common occurrence. Figures S1 and S2 highlight the similarities of the WT plots for the first metal shell of all 24 Ni-rich mineral standards. Often it is not possible to distinguish based on the WT alone if the sample is an LDH or a single metal hydroxide. Except for the cases of β-Ni(OH)$_2$, there are generally two components in the WT of the single metal hydroxides.

As a result of the similarities of the WT plots, for these samples, WT of the first metal shell should not be used to identify an LDH because the spectra of single metal hydroxides and silicate standards are indistinguishable from the LDH. Two components are identified by WT for LDHs, most layered single metal hydroxides, and the metal silicates. This disproved the hypothesis that the first metal shell for all Ni(OH)$_2$ phases should contain just one major component. There is another component apart from Ni that contributes to the EXAFS spectrum. The effect of an adsorbed interlayer anion, however, does not significantly alter the Ni−Ni path of the shell fitting results of the RSF, as the Ni−Ni distance is still further apart in the single metal hydroxides than in the LDHs (Table S1).

3.4. Third Metal Shell Differences. Figures S3 and S4 are the WT plots of the third metal shell of all 24 mineral standards. If the WT of the first metal shell cannot reliably be used to distinguish between single metal hydroxides and LDHs, perhaps the third metal shell can provide some discrimination between the minerals. The second and third metal shells result from focused multiple scattering in the hydroxide sheet,[5,20] and thus it is hypothesized those shells should not be influenced by adsorbed anions to the extent of the first metal shell. The adsorbed anions do not have the linear, focused multiple scattering that is found in the octahedral layer. The second metal shell of the LDH is composed of only Ni atoms, while the third metal shell is composed of Ni and Al atoms (Figure S7).[20]

Emphasis in Figures S3 and S4 is placed on the 7−10.3 Å^{-1} *k*-range (as discussed in Figure S5). Results of WT using a variety of σ values indicate that σ = 0.17 and below suffice to separate the third metal shell into its two components, the lighter Al component at lower *k* (ca. 8.8 Å^{-1}) and the heavier Ni component at higher *k* (ca. 9.9 Å^{-1}). Different values have been used in the literature where η = 30 and σ = 0.155;[20] however, as shown in Figure S5, this value and lower values of σ are not required to show discrete Ni and Al components in the third shell.

As hypothesized, two major components are identified for the WT of the third metal shells of the LDHs (Figure S3), except for LDH #6 which contains one major and one minor component. These two components can be ascribed to metals in a similar fashion as the first metal shell, with Al being the lower energy component and Ni being the higher component. The LDH-silicates also have two components in the third metal shell, which is expected because they both have Ni and Al in their hydroxide sheets. However, Ni silicate #1 also has two components, which was not expected because this sample has just one metal in the hydroxide sheet (Figure S6). This could potentially be caused by contribution of the Si tetrahedral sheet. The WT of the Ni silicate #2 does not show substantial contribution from the third metal shell. The "LDH-py" sample has two major components, which is expected because this sample is an LDH,[9] with potentially Si in the interlayer. Lastly, the Ni basic nitrate,[33] albeit with a minor component, has just one major component from the third metal shell, which is expected because it contains only one metal type in the hydroxide sheet.

When Figure S3 (LDHs) is compared to Figure S4 (single metal hydroxides), in general there is only one major component in the WT of the Ni(OH)$_2$ standards. One dominant component is present in all Ni(OH)$_2$ standards except #3, which may be due to a comparatively small third metal shell in the RSF (Figure 1b). Of the other standards, minor secondary components are present in the WT plots in #1, #4, #6, #8, #9, and #11. These secondary components are mainly present in the more disordered α-Ni(OH)$_2$ phases.

Distinction between α- and β-phases of Ni(OH)$_2$ can be made by looking at the EXAFS data (Figure 1a), where the β-phases exhibit well-defined doublet peaks at ca. 7 Å^{-1} and 8 Å^{-1}. Particularly, β-Ni(OH)$_2$ #5, #10, and #12 have the most pronounced doublet peaks; they were each prepared explicitly as the β-phase. Additionally, their WT plots are similar in shape with no substantial secondary components (Figure S2). α-Ni(OH)$_2$ spectra (including α-Ni(OH)$_2$ #1, #6, #7, and #8) exhibit less pronounced doublet peaks at ca. 7 Å^{-1} and 8 Å^{-1};

DOI: 10.1021/acs.jpca.7b07940
J. Phys. Chem. A XXXX, XXX, XXX−XXX

however, their WT plots still display two components (Figure S2). The major differences between the α- and β-$Ni(OH)_2$ is that the β-phase is well crystallized while the α-phase is disordered (poorly crystallized) and water layers are present between the sheets.[15,33] Additionally, the c-axis is increased to about 8 Å in the α-phase versus 4.6 Å in the β-phase. Increased focused multiple scattering will occur in the more crystalline standards, thus yielding more intense third metal shells and WT plots with just one significant component.

Determining metal cation locations in LDHs is difficult because a high degree of order (i.e., crystallinity) is often not obtained during synthesis.[36] LDHs can be amorphous and remain amorphous when they form on phyllosilicates minerals. Crystalline peaks of Ni−Al LDH were not observed using high resolution transmission electron microscopy (HRTEM) and powder X-ray diffraction (PXRD) even after five years of reaction time for a Ni-pyrophyllite system ("LDH-py" in this work). Ni is locally ordered as LDH, but there is no long-range crystallinity of LDH. Silication of the interlayer can inhibit the formation of crystalline LDH.[9] Other reaction conditions (e.g., using Si-free sorbents) can facilitate precipitation of LDH nanocrystals.[13]

3.5. Fingerprinting LDHs. If LDHs and Ni/Zn-rich phyllosilicates commonly contain both heavy and light elements, such as Ni or Zn and Mg or Al, then a diagnostic feature should be a split in the first oscillation of the EXAFS data at 3.8 $Å^{-1}$. The local atomic environment of Ni atoms is very similar in both mineral types, with the nearest cation neighbor to Ni or Zn being Mg or Al in an octahedral layer.[37] This split is commonly present in many Ni and Zn bearing phyllosilicates (e.g., lizardite).[37,38] The appearance of this shoulder/split can be used to "fingerprint" this type of octahedrally coordinated structural environment common to LDHs, silicated LDHs, and metal-rich phyllosilicates.[39−43] However, most Ni−Al LDHs do not have the splitting peak of the first EXAFS oscillation at 3.8 $Å^{-1}$ (e.g., see ref 4).

The reason, as clarified in ref 37, is because in metal-rich LDHs and metal-rich phyllosilicates, the metal (e.g., Ni or Zn) is surrounded by both light (Al or Mg) and heavy atoms (Ni or Zn), which causes the split to disappear.[37,44] In layered silicates, such as lizardite, there is a dominance of Mg distribution around Ni atoms, thus the split and/or shoulder is clear.[38] Further discussion on the split of the first oscillation can be found in the references.[34,45,46]

Apart from the split in the peak of the first EXAFS oscillation, the LDH can also be fingerprinted by the presence of a beat pattern. An EXAFS beat pattern at ca. 8 $Å^{-1}$ can distinguish the LDH from the single metal hydroxides and phyllosilicates (Figure S8).[16] In Figure S8a, the beat pattern at ca. 8 $Å^{-1}$ is present in both LDH #2 and LDH #3. In LDH #2, the Ni:Al ratio is 1.3, and in LDH #3, the Ni:Al ratio is 4.3. There is a truncation in the peak between 8−8.5 $Å^{-1}$ in the LDH spectra versus the α-$Ni(OH)_2$. When a FT is applied to these spectra, the amplitude of the first metal shell decreases (Figure S8b). This decrease is the effect of Al substitution into the hydroxide sheet. With increasing Al substitution, the amplitude decreases further (LDH #2 versus LDH #3). This effect is caused by deconstructive interference of the back-scattering photoelectric waves of Ni and Al, which are out of phase to each other.[16,17,33]

This destructive interference is illustrated in Figure S8c, where scattering paths for Ni, Al, and Si are presented for LDH silicate #1. The addition of the Ni and Al scattering waves will effectively decrease the amplitude of the first metal shell in the FT. The scattering path for Ni is out of phase with Al and in phase with Si.

4. CONCLUSIONS

In the samples analyzed it was not possible to distinguish between LDHs and α-$Ni(OH)_2$ for almost all standards using WT because their WT plots of the first metal shells were indistinguishable from each other (Figure 3 and Figures S1 and S2). Two components were identified in the first metal shell WT plots of the LDHs, α-$Ni(OH)_2$, and metal silicates. Thus, for these samples, WT of the first metal shell should not be used to identify LDHs because the plots are indistinguishable. WT was able to expose that many of the α-$Ni(OH)_2$ standards actually have two significant scattering components in the first metal shell of the RSF. A comparison to a Ni basic nitrate standard confirmed that the intensity of the second component is increased with the presence of adsorbed interlayer anions. Thus, adsorbed anions to the hydroxide layer can affect the EXAFS spectra and are not visible in the FT but clearly resolved and discrete in the WT. A slight reduction in the amplitude of the EXAFS oscillations is present in the Ni basic nitrate standard versus the α-$Ni(OH)_2$ (Figure 1).

Differences in third metal shell WT plots of $Ni(OH)_2$ and LDH standards are more pronounced than in first metal shell WT plots because the third metal shell results from focused, linear multiple scattering in the hydroxide sheet and is less affected by adsorbed anions. Major and minor secondary components were common for α-$Ni(OH)_2$ standards in the first and third metal shell WT plots, respectively, while β-$Ni(OH)_2$ standards consistently displayed only one component. Silicated minerals, such as Ni-phyllosilicate, can also display two components in the third metal shell WT plot, similarly to the LDHs. This second component may be caused by the tetrahedral layer of Si. Thus, it was not possible to distinguish between a Ni phyllosilicate and a Ni−Al LDH using WT of the third metal shell.

Minor secondary components present in the third metal shell WT plots of α-$Ni(OH)_2$ are difficult to assign to a particular scattering component. They can also be similar to minor components in third metal shell WT plots of LDHs (e.g., in Figure S4, α-$Ni(OH)_2$ #9 and #11 are similar to LDH WT plots in Figure S3). Minor secondary scattering components could be common in geochemical mineral systems, such as soils and sediments, where LDHs can remain amorphous and α-$Ni(OH)_2$ can have considerable vacancy sites during formation;[9,16,34] however, they are also present here in the well characterized α-$Ni(OH)_2$ #9 and #11 standards. WT will not differentiate between Al and Si when they are present in the same coordination shell because they are both very similar in atomic weight. The similarities in WT plots (Figures S1−S4) make it difficult to use WT alone to attribute the second component at lower energy to the presence of Al in an LDH that is forming in a natural geochemical system.

■ ASSOCIATED CONTENT

Supporting Information

The Supporting Information is available free of charge on the ACS Publications website at DOI: 10.1021/acs.jpca.7b07940.

Structural parameters of previously unpublished EXAFS spectra; first and third metal shell WT plots of all the spectra; effects of σ and η parameters on second and

DOI: 10.1021/acs.jpca.7b07940
J. Phys. Chem. A XXXX, XXX, XXX−XXX

third metal shells WT; structural models layered Ni- and Al-rich minerals; Ni−Al LDH sheet illustrating coordination shells and multiple scattering; EXAFS comparison of LDHs to α-Ni(OH)$_2$(PDF)

AUTHOR INFORMATION

Corresponding Author

*E-mail: mgs@udel.edu. Tel.: 1-302-831-8435.

ORCID

Matthew G. Siebecker: 0000-0002-1348-6543

Notes

The authors declare no competing financial interest.

ACKNOWLEDGMENTS

This publication was made possible by the National Science Foundation EPSCoR Grants No. IIA-1301765 and EPS-0814251 and the State of Delaware. Any opinions, findings, and conclusions or recommendations expressed in this material are those of the author(s) and do not necessarily reflect the views of the National Science Foundation. Use of the NSLS was supported by the US Department of Energy under contract No. DE-AC02-98CH10886. The following people are acknowledged for spectral contributions or helpful discussions: Ryan Tappero, David McNear, Ted Peltier, Andreas Scheinost, and Marina Chukalina.

REFERENCES

(1) Forano, C.; Hibino, T.; Leroux, F.; Taviot-Gueho, C. In *Handbook of Clay Science*; Bergaya, F., Theng, B. K. G., Lagaly, G., Eds; Elsevier Science Bv: Amsterdam, 2006; Vol. *1*, pp 1021−1095.

(2) *Layered Double Hydroxides: Present and Future*; Rives, V., Ed; Nova Science Publishers, Inc.: New York, 2001.

(3) Allada, R. K.; Peltier, E.; Navrotsky, A.; Casey, W. H.; Johnson, C. A.; Berbeco, H. T.; Sparks, D. L. Calorimetric determination of the enthalpies of formation of hydrotalcite-like solids and their use in the geochemical modeling of metals in natural waters. *Clays Clay Miner.* **2006**, *54*, 409−417.

(4) Peltier, E.; Allada, R.; Navrotsky, A.; Sparks, D. L. Nickel solubility and precipitation in soils: a thermodynamic study. *Clays Clay Miner.* **2006**, *54*, 153−164.

(5) Siebecker, M.; Li, W.; Khalid, S.; Sparks, D. Real-time QEXAFS spectroscopy measures rapid precipitate formation at the mineral−water interface. *Nat. Commun.* **2014**, *5*, 5003.

(6) Peltier, E.; Lelie, D. v. d.; Sparks, D. L. Formation and stability of Ni−Al hydroxide phases in soils. *Environ. Sci. Technol.* **2010**, *44*, 302−308.

(7) Shi, Z.; Peltier, E.; Sparks, D. L. Kinetics of Ni sorption in soils: roles of soil organic matter and Ni precipitation. *Environ. Sci. Technol.* **2012**, *46*, 2212−2219.

(8) McNear, D. H.; Chaney, R. L.; Sparks, D. L. The effects of soil type and chemical treatment on nickel speciation in refinery enriched soils: A multi-technique investigation. *Geochim. Cosmochim. Acta* **2007**, *71*, 2190−2208.

(9) Livi, K. J. T.; Senesi, G. S.; Scheinost, A. C.; Sparks, D. L. Microscopic examination of nanosized mixed Ni-Al hydroxide surface precipitates on pyrophyllite. *Environ. Sci. Technol.* **2009**, *43*, 1299−1304.

(10) Nachtegaal, M.; Marcus, M. A.; Sonke, J. E.; Vangronsveld, J.; Livi, K. J. T.; Van der Lelie, D.; Sparks, D. L. Effects of in situ remediation on the speciation and bioavailability of zinc in a smelter contaminated soil. *Geochim. Cosmochim. Acta* **2005**, *69*, 4649−4664.

(11) Starcher, A. N.; Li, W.; Kukkadapu, R. K.; Elzinga, E. J.; Sparks, D. L. Fe(II) sorption on pyrophyllite: Effect of structural Fe(III) (impurity) in pyrophyllite on nature of layered double hydroxide (LDH) secondary mineral formation. *Chem. Geol.* **2016**, *439*, 152−160.

(12) Thompson, H. A.; Parks, G. A.; Brown, G. E. Dynamic interactions of dissolution, surface adsorption, and precipitation in an aging cobalt(II)-clay-water system. *Geochim. Cosmochim. Acta* **1999**, *63*, 1767−1779.

(13) Li, W.; Livi, K. J. T.; Xu, W. Q.; Siebecker, M. G.; Wang, Y. J.; Phillips, B. L.; Sparks, D. L. Formation of crystalline Zn-Al layered double hydroxide precipitates on gamma-alumina: the role of mineral dissolution. *Environ. Sci. Technol.* **2012**, *46*, 11670−11677.

(14) Elzinga, E. J. Formation of layered Fe(II)-Al(III)-hydroxides during reaction of Fe(II) with aluminum oxide. *Environ. Sci. Technol.* **2012**, *46*, 4894−4901.

(15) Pandya, K. I.; O'Grady, W. E.; Corrigan, D. A.; McBreen, J.; Hoffman, R. W. Extended X-ray absorption fine-structure investigations of nickel hydroxides. *J. Phys. Chem.* **1990**, *94*, 21−26.

(16) Scheinost, A. C.; Sparks, D. L. Formation of layered single- and double-metal hydroxide precipitates at the mineral/water interface: a multiple-scattering XAFS analysis. *J. Colloid Interface Sci.* **2000**, *223*, 167−178.

(17) Manceau, A. Distribution of cations among the octahedra of phyllosilicates - insight from EXAFS. *Can. Mineral.* **1990**, *28*, 321−328.

(18) Funke, H.; Scheinost, A. C.; Chukalina, M. Wavelet analysis of extended X-ray absorption fine structure data. *Phys. Rev. B: Condens. Matter Mater. Phys.* **2005**, *71*, 094110.

(19) Aimoz, L.; Taviot-Gueho, C.; Churakov, S. V.; Chukalina, M.; Dahn, R.; Curti, E.; Bordet, P.; Vespa, M. Anion and cation order in iodide-bearing Mg/Zn-Al layered double hydroxides. *J. Phys. Chem. C* **2012**, *116*, 5460−5475.

(20) Funke, H.; Chukalina, M.; Scheinost, A. C. A new FEFF-based wavelet for EXAFS data analysis. *J. Synchrotron Radiat.* **2007**, *14*, 426−432.

(21) Zhu, Y.; Elzinga, E. J. Formation of layered Fe(II)-hydroxides during Fe(II) sorption onto clay and metal-oxide substrates. *Environ. Sci. Technol.* **2014**, *48*, 4937−4945.

(22) Mikutta, C.; Frommer, J.; Voegelin, A.; Kaegi, R.; Kretzschmar, R. Effect of citrate on the local Fe coordination in ferrihydrite, arsenate binding, and ternary arsenate complex formation. *Geochim. Cosmochim. Acta* **2010**, *74*, 5574−5592.

(23) Karlsson, T.; Persson, P.; Skyllberg, U.; Morth, C. M.; Giesler, R. Characterization of iron(III) in organic soils using extended X-ray absorption fine structure spectroscopy. *Environ. Sci. Technol.* **2008**, *42*, 5449−5454.

(24) Ravel, B.; Newville, M. ATHENA, ARTEMIS, HEPHAESTUS: data analysis for X-ray absorption spectroscopy using Ifeffit. *J. Synchrotron Radiat.* **2005**, *12*, 537−541.

(25) Huwaldt, J. A.; Steinhorst, S. *Plot Digitizer*, version 2.6.8; jhuwaldt, http://plotdigitizer.sourceforge.net, 2015.

(26) Ford, R. G.; Scheinost, A. C.; Scheckel, K. G.; Sparks, D. L. The link between clay mineral weathering and the stabilization of Ni surface precipitates. *Environ. Sci. Technol.* **1999**, *33*, 3140−3144.

(27) Khalid, S.; Caliebe, W.; Siddons, P.; So, I.; Clay, B.; Lenhard, T.; Hanson, J.; Wang, Q.; Frenkel, A. I.; Marinkovic, N.; et al. Quick extended X-ray absorption fine structure instrument with millisecond time scale, optimized for in situ applications. *Rev. Sci. Instrum.* **2010**, *81*, 015105.

(28) Genin, P.; Delahayevidal, A.; Portemer, F.; Tekaiaelhsissen, K.; Figlarz, M. Preparation and characterization of alpha-type nickel hydroxides obtained by chemical precipitation - study of the anionic species. *Eur. J. Solid State Inorg. Chem.* **1991**, *28*, 505−518.

(29) Taylor, R. M. The rapid formation of crystalline double hydroxy salts and other compounds by controlled hydrolysis. *Clay Miner.* **1984**, *19*, 591−603.

(30) Chukalina, M.; Funke, H. *Wavelet Transform for EXAFS*, version Wavelet2.ipf; The European Synchrotron, www.esrf.eu/UsersAndScience/Experiments/CRG/BM20/Software/Wavelets, 2013.

(31) Scheinost, A. C.; Kirsch, R.; Banerjee, D.; Fernandez-Martinez, A.; Zaenker, H.; Funke, H.; Charlet, L. X-ray absorption and

DOI: 10.1021/acs.jpca.7b07940
J. Phys. Chem. A XXXX, XXX, XXX−XXX

photoelectron spectroscopy investigation of selenite reduction by FeII-bearing minerals. *J. Contam. Hydrol.* **2008**, *102*, 228−245.
(32) Starcher, A. N.; Elzinga, E. J.; Sparks, D. L. Formation of a mixed Fe(II)-Zn-Al layered hydroxide: Effects of Zn co-sorption on Fe(II) layered hydroxide formation and kinetics. *Chem. Geol.* **2017**, *464*, 46−56.
(33) d'Espinose de la Caillerie, J. B.; Kermarec, M.; Clause, O. Impregnation of gamma-alumina with Ni(II) or Co(II) ions at neutral pH - hydrotalcite-type coprecipitate formation and characterization. *J. Am. Chem. Soc.* **1995**, *117*, 11471−11481.
(34) Siebecker, M.; Li, W.; Sparks, D. The important role of layered double hydroxides in soil chemical processes and remediation: What we have learned over the past 20 years. *Advances in Agronomy*; Elsevier, 2017; Vol. *147*, in press.
(35) Charlet, L.; Manceau, A. Evidence for the neoformation of clays upon sorption of Co(II) and Ni(II) on silicates. *Geochim. Cosmochim. Acta* **1994**, *58*, 2577−2582.
(36) Costa, D. G.; Rocha, A. B.; Diniz, R.; Souza, W. F.; Chiaro, S. S. X.; Leitao, A. A. Structural model proposition and thermodynamic and vibrational analysis of hydrotalcite-like compounds by DFT calculations. *J. Phys. Chem. C* **2010**, *114*, 14133−14140.
(37) Manceau, A.; Marcus, M. A.; Tamura, N.; Proux, O.; Geoffroy, N.; Lanson, B. Natural speciation of Zn at the micrometer scale in a clayey soil using X-ray fluorescence, absorption, and diffraction. *Geochim. Cosmochim. Acta* **2004**, *68*, 2467−2483.
(38) Siebecker, M. G.; Chaney, R. L.; Sparks, D. L. Nickel speciation in several serpentine (ultramafic) topsoils via bulk synchrotron-based techniques. *Geoderma* **2017**, *298*, 35−45.
(39) Manceau, A.; Llorca, S.; Calas, G. Crystal-chemistry of cobalt and nickel in lithiophorite and asbolane from New-Caledonia. *Geochim. Cosmochim. Acta* **1987**, *51*, 105−113.
(40) Manceau, A.; Schlegel, M. L.; Musso, M.; Sole, V. A.; Gauthier, C.; Petit, P. E.; Trolard, F. Crystal chemistry of trace elements in natural and synthetic goethite. *Geochim. Cosmochim. Acta* **2000**, *64*, 3643−3661.
(41) Roberts, D. R.; Scheinost, A. C.; Sparks, D. L. Zinc speciation in a smelter-contaminated soil profile using bulk and microspectroscopic techniques. *Environ. Sci. Technol.* **2002**, *36*, 1742−1750.
(42) Roberts, D. R.; Ford, R. G.; Sparks, D. L. Kinetics and mechanisms of Zn complexation on metal oxides using EXAFS spectroscopy. *J. Colloid Interface Sci.* **2003**, *263*, 364−376.
(43) Scheinost, A. C.; Kretzschmar, R.; Pfister, S.; Roberts, D. R. Combining selective sequential extractions, X-ray absorption spectroscopy, and principal component analysis for quantitative zinc speciation in soil. *Environ. Sci. Technol.* **2002**, *36*, 5021−5028.
(44) Schlegel, M. L.; Manceau, A.; Charlet, L.; Hazemann, J.-l. Adsorption mechanisms of Zn on hectorite as a function of time, pH, and ionic strength. *Am. J. Sci.* **2001**, *301*, 798−830.
(45) Nachtegaal, M.; Scheidegger, A. M.; Dähn, R.; Chateigner, D.; Furrer, G. Immobilization of Ni by Al-modified montmorillonite: A novel uptake mechanism. *Geochim. Cosmochim. Acta* **2005**, *69*, 4211−4225.
(46) Schlegel, M. L.; Manceau, A. Zn incorporation in hydroxy-Al- and Keggin Al-13-intercalated montmorillonite: A powder and polarized EXAFS study. *Environ. Sci. Technol.* **2007**, *41*, 1942−1948.

DOI: 10.1021/acs.jpca.7b07940
J. Phys. Chem. A XXXX, XXX, XXX−XXX

Supporting Information for:

Structural Differentiation Between Layered Single (Ni) and Double Metal Hydroxides (Ni-Al LDH) Using Wavelet Transformation

Authorship: Matthew G Siebecker*,[1] and Donald L Sparks[1]

Affiliation: [1]University of Delaware, Delaware Environmental Institute (DENIN), Interdisciplinary Science and Engineering (ISE) Laboratory, 221 Academy Street, Newark, DE, 19716

*Correspondence to: E-mail: mgs@udel.edu ; Phone: 1-302- 831-8435

CONTENTS:

TABLES

FIGURES

REFERENCES

Table S1. EXAFS structural parameters (see Table 1 references for all other spectra). **R factor** is the absolute misfit between data and theory employed in Artemis [1], $R = [\Sigma(data - fit^2)]/[\Sigma(data^2)]$; **CN** is the coordination number; **R** is the interatomic distance in Å; $\boldsymbol{\sigma^2}$ is the Debye–Waller factor in $Å^2$; **ΔE** is the energy shift in eV; $\boldsymbol{S_0^2}$ is the amplitude reduction factor and was set to 0.9. The CN uncertainty value (**±CN**) includes an additional 15% added in quadrature to the value calculated by the fitting algorithm to account for fixing S_0^2 to 0.9 [2]. A Hanning window was used for both the forward (dk=1) and back (dR =0.5) Fourier transformation. All spectra were fit with a k weighting of 3. Crystal Information Files (CIF) were used as models for scattering paths included theophrastite [3] for the nickel hydroxides and lizardite [4] for the Ni-Al LDH. Two fits are presented from the LDH, with and without the inclusion of the Al scattering path. For the LDH fit, ΔR and σ^2 were restricted to be the same value.

Sample	R-factor	Path	CN	R (Å)	$\sigma^2(Å^2)$ $x10^{-3}$	ΔE (eV)	±CN	±R (Å)	$\pm\sigma^2(Å^2)$ $x10^{-3}$	±ΔE (eV)
$Ni(OH)_2$ #1	0.005	Ni-O	6.2	2.068	6	1.0	1.0	0.005	1	0.5
		Ni-Ni	6.9	3.127	7	1.0	1.3	0.004	1	0.5
$Ni(OH)_2$ #3	0.018	Ni-O	5.5	2.061	7	0.8	1.0	0.012	2	0.9
		Ni-Ni	8.4	3.115	12	0.8	2.8	0.012	3	0.9
$Ni(OH)_2$ #4	0.010	Ni-O	5.2	2.066	7	0.6	0.9	0.009	1	0.7
		Ni-Ni	6.1	3.128	9	0.6	1.6	0.008	2	0.7
$Ni(OH)_2$ #7	0.008	Ni-O	6.0	2.080	6	1.1	1.0	0.010	2	0.7
		Ni-Ni	6.3	3.144	7	1.1	1.6	0.009	2	0.7
$Ni(OH)_2$ #8	0.008	Ni-O	5.3	2.071	6	1.0	0.9	0.008	1	0.6
		Ni-Ni	6.3	3.129	7	1.0	1.3	0.006	1	0.6
LDH #5	0.008	Ni-O	6.0	2.062	6	0.6	1.1	0.008	1	0.8
		Ni-Ni	4.6	3.061	8	0.6	2.0	0.010	3	0.8
		Ni-Al	1.2	3.061	8	0.6	1.3	0.010	3	0.8
	0.010	Ni-O	5.6	2.061	6	0.79	0.9	0.008	1	0.7
		Ni-Ni	3.2	3.065	6	0.79	1.0	0.009	2	0.7

Figure S1. First metal shell WT plots of Ni-Al LDH and Ni-rich silicate spectra. WT parameters (η and σ) were kept the same for all WT (η= 30, σ=0.18) and optimized for the first metal shell distance (η·σ≈2·r, where r is the distance of interest) [5].

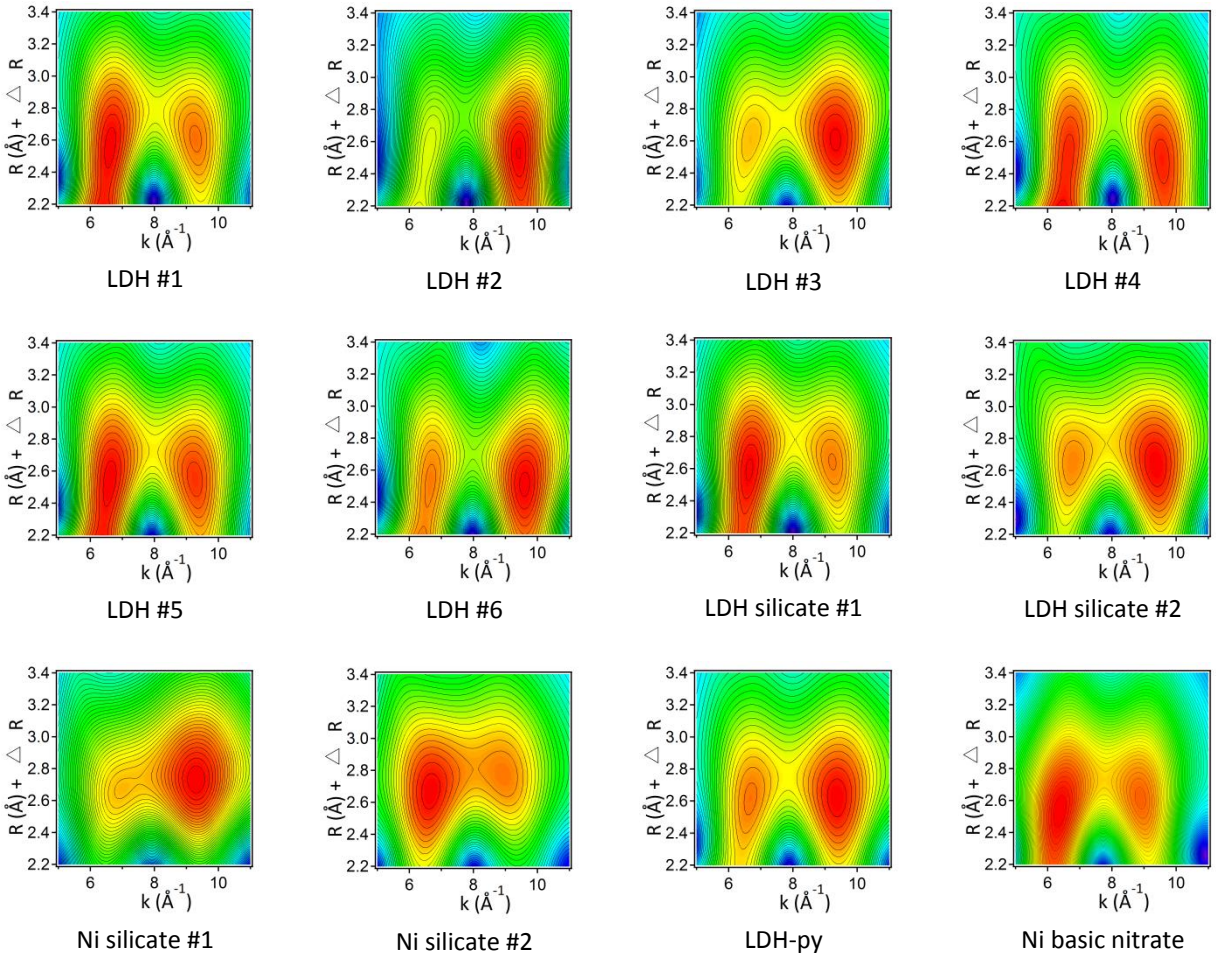

Figure S2. First metal shell WT plots of $Ni(OH)_2$ spectra. WT parameters (η and σ) were kept the same for all WT (η= 30, σ=0.18) and optimized for the first metal shell distance (η·σ≈2·r, where r is the distance of interest) [5].

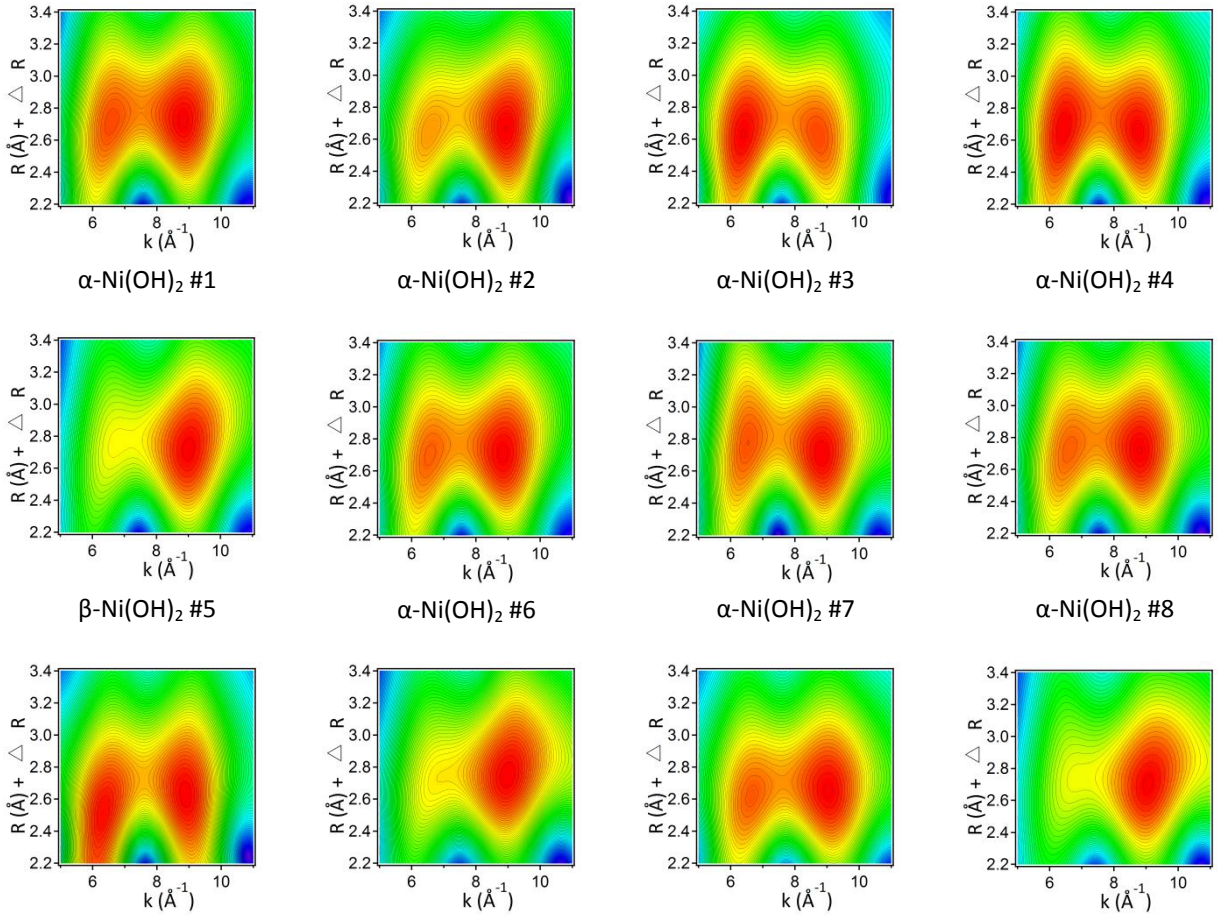

Figure S3. Third metal shells WT plots of Ni-Al LDH and Ni-rich silicate spectra. WT parameters (η and σ) were kept the same for all WT (η= 30, σ=0.17) and optimized for the third metal shell distance determined in Figure S5.

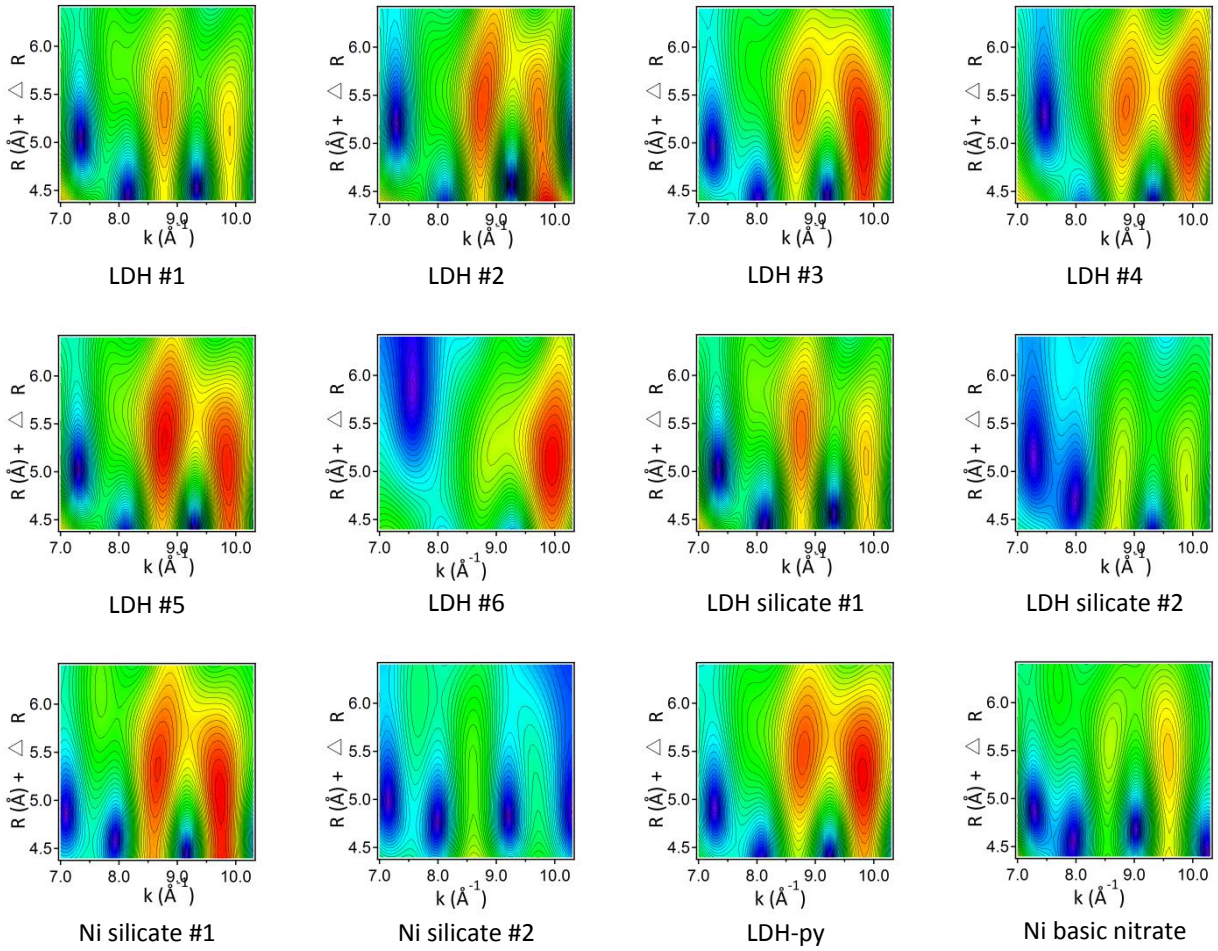

Figure S4. Third metal shells WT plots of $Ni(OH)_2$ spectra. WT parameters (η and σ) were kept the same for all WT (η= 30, σ=0.17) and optimized for the third metal shell distance determined in Figure S5.

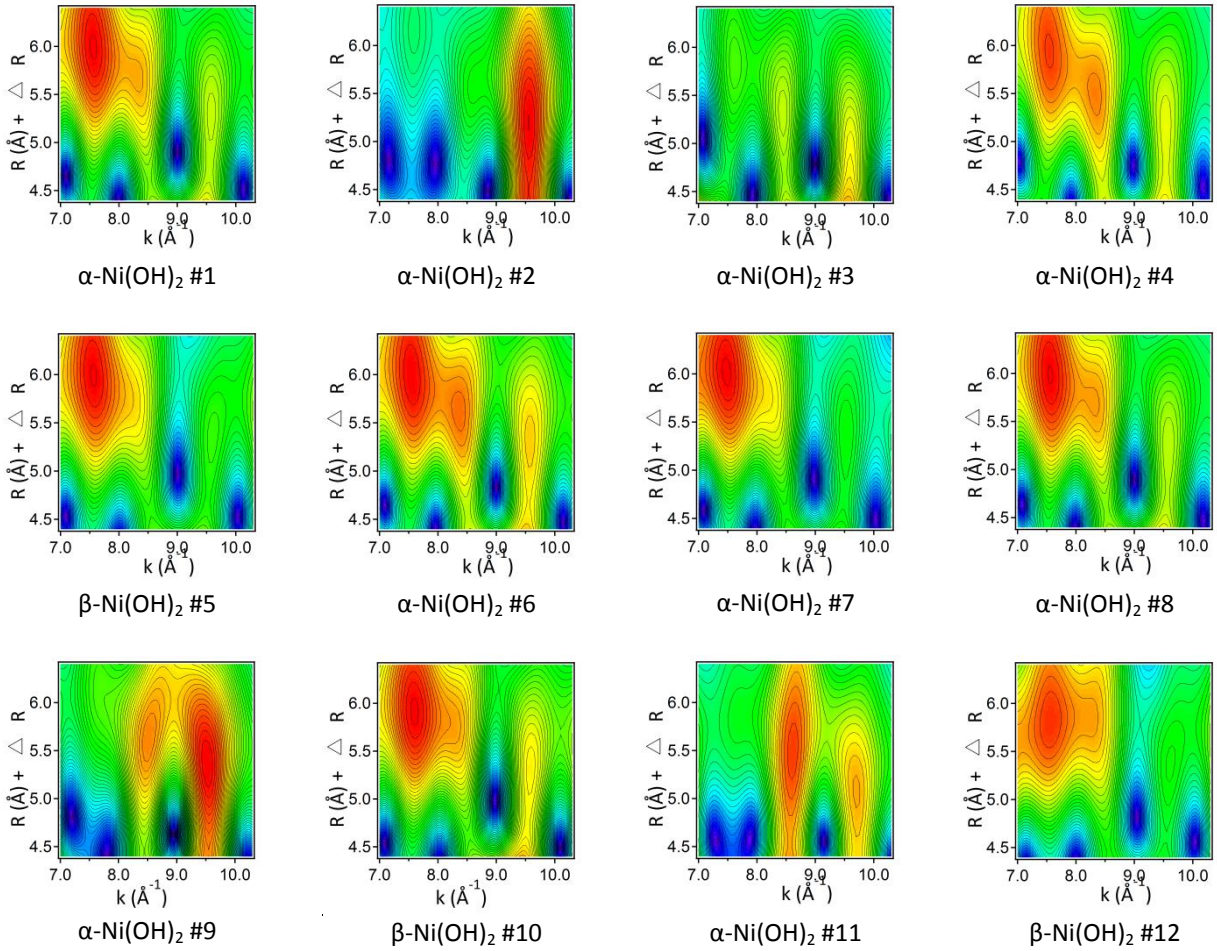

Figure S5. WT plots illustrating the effect of changes to the eta (η) and sigma (σ) parameters on the second and third metal shells of LDH #4. In this series of plots, η remains constant while σ is varied from 1 to 0.14. At σ=1, resolution in R-space is high while resolution in k-space is low (maximum spatial resolution in r-space) [6]. The second and third metal shell maxima are clearly resolved at σ=1, with the second metal shell having a maximum at ca k = 7 $Å^{-1}$ and the third metal shell with a maximum at k = 9 $Å^{-1}$. Ideally the WT maximum of the third metal shell in the LDH should be at a lower k-value than the second metal shell [7]. However, an increase in the Me^{2+}/Me^{3+} ratio in the third metal shell can prevent this distinction [8]. As σ is decreased to 0.14 a gradual shift in the second metal shell can be seen towards lower k values and the third metal shell begins to split at σ=0.23. As σ decreases a slow transition of maxima in the second and third metal shells can be seen as a clockwise rotation until ca σ=0.23, where the maxima begin to separate into separate peaks. At lower σ values resolution is optimized for k-space. At σ=0.17 and lower σ values, the k-range in the plot is decreased to include only third metal shell maxima and this is the range used for all other plots of the third metal shell.

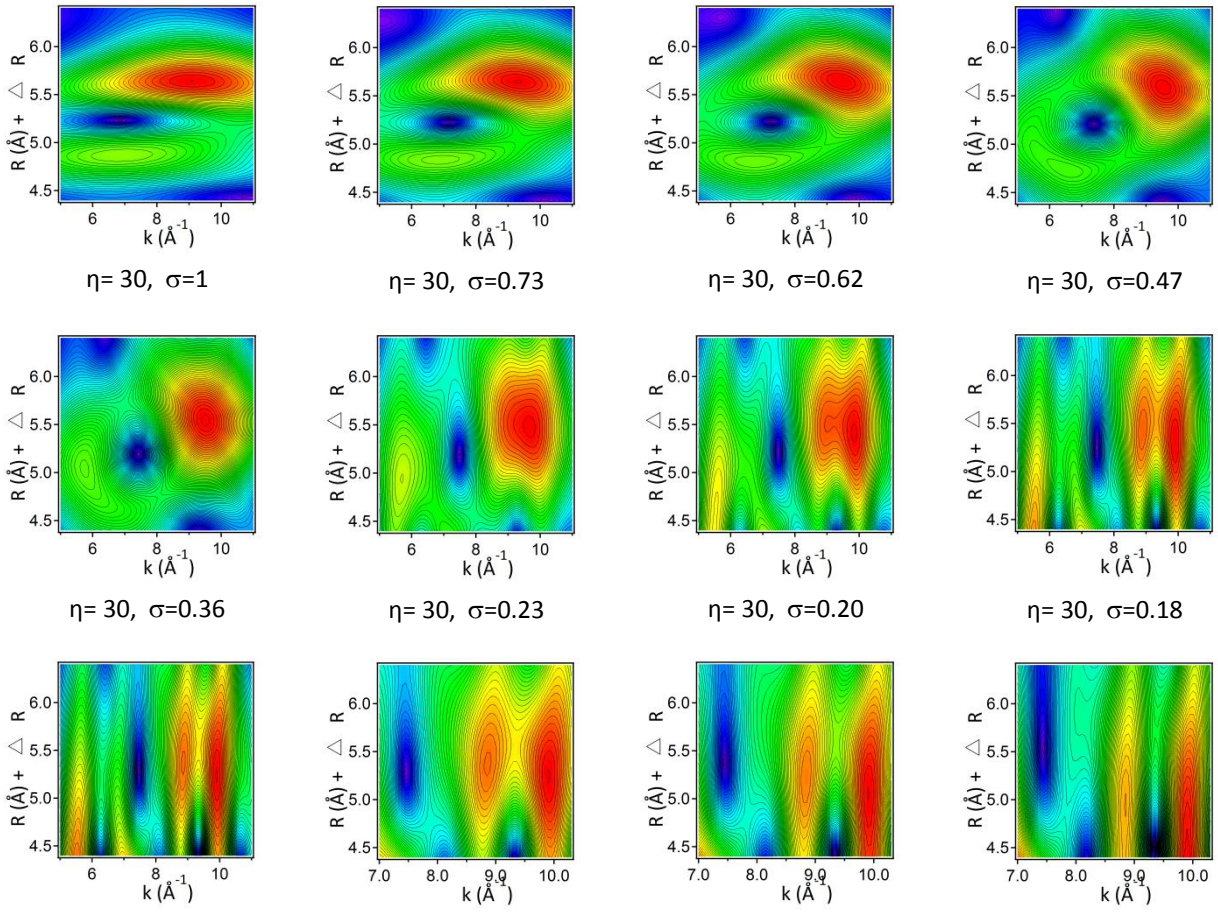

Figure S6. Structural models of Ni-rich and related layered minerals. Atoms and polyhedra are as follows: oxygen (red), nickel (green), aluminum (light blue), silicon (dark blue), and were created using the VESTA visualization software [9]. Hydrogen atoms have been removed for clarity. Top and side views are presented with no interlayer anions. CIF files were used to create the Ni-Al LDH [10], $Ni(OH)_2$ [3], gibbsite [11], Ni-Al-phyllosilicate [12], Ni-phyllosilicate [12], and kaolinite [13] models. Nickel atoms were substituted for Mg in the hydrotalcite structure to create the Ni-Al LDH. Nickel atoms were substituted for Mg in the lizardite structure to create the Ni-phyllosilicate and subsequently Al atoms for Ni to create the Ni-Al phyllosilicate. Ni-rich layered minerals are similar in structure to many common soil clay minerals such a gibbsite and kaolinite, both having octahedral and/or tetrahedral stacking layers.

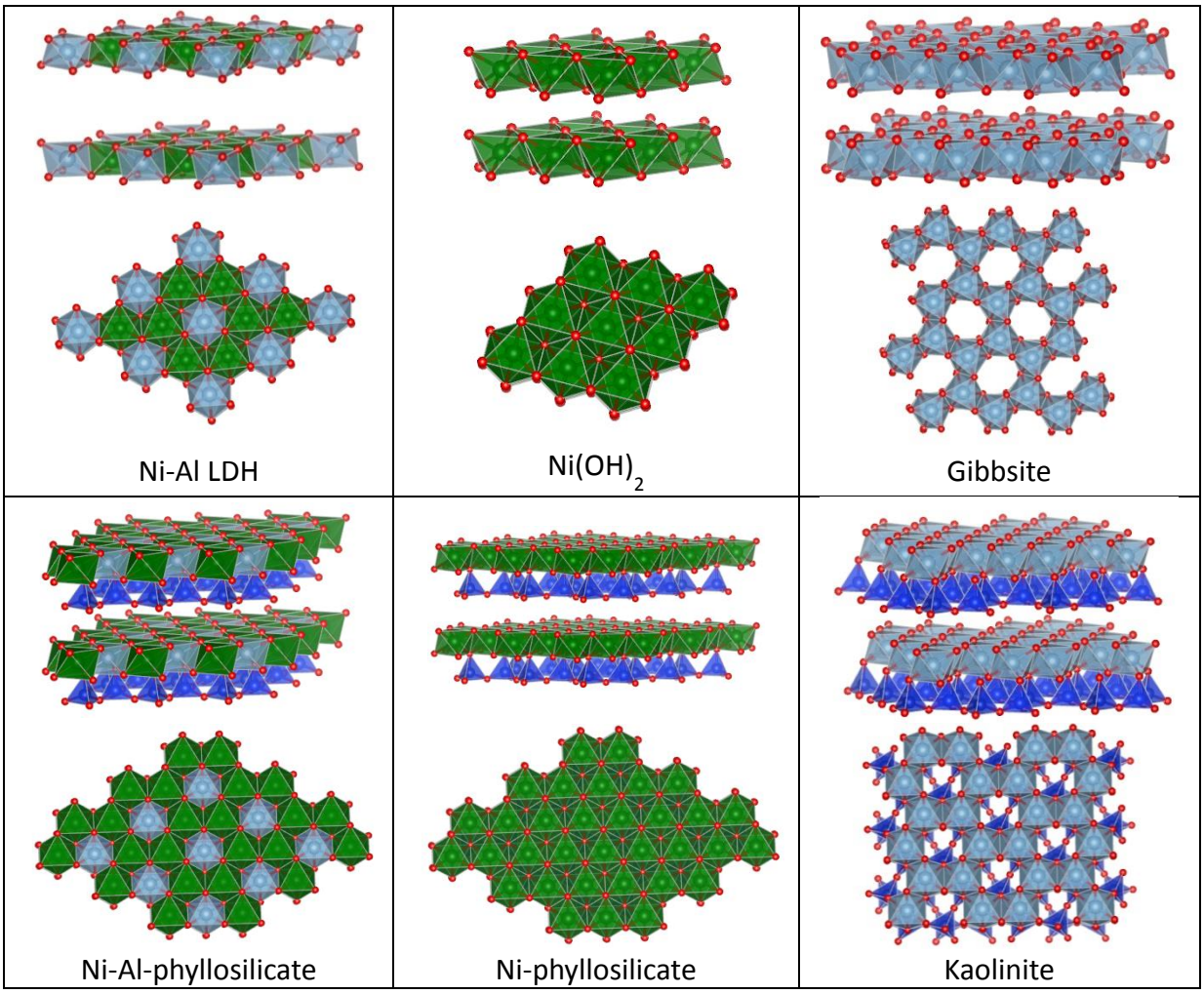

Figure S7. The hydroxide layer of Ni-Al LDH from above. In the CIF file for hydrotalcite [10] Ni was substituted for Mg. This view from above illustrates the coordination shells around a central absorbing Ni atom. The innermost yellow circle is the first coordination shell of 6 oxygen atoms (red). The second yellow circle from the middle is the ***first*** metal shell. It is a mixed metal shell containing both nickel (green) and aluminum (blue) atoms. The outer two yellow circles are the second and third metal shells, with the outermost yellow circle being the ***third metal shell***. The second metal shell circle passes through only Ni atoms while the third metal shell passes through both Ni and Al atoms. Thus the second metal shell consists of a single metal while the third metal shell is a mixed metal shell. The black arrows indicate a focused forward multiple scattering path that is an example of what causes the significant amplitude for the third metal shell. Although a 2:1 LDH structure is fully (globally) ordered in a honeycomb fashion where no Al^{3+}-Al^{3+} are in close contact (i.e., Al-Al pairs are avoided) and at lower Al content there is still a nonrandom distribution of cations [14], a small fraction of Al atoms can be misplaced and detectable amounts of Al clustering can be measured [15]. This figure was reproduced (adapted) from reference 7 with permission from the International Union of Crystallography (click link to follow).

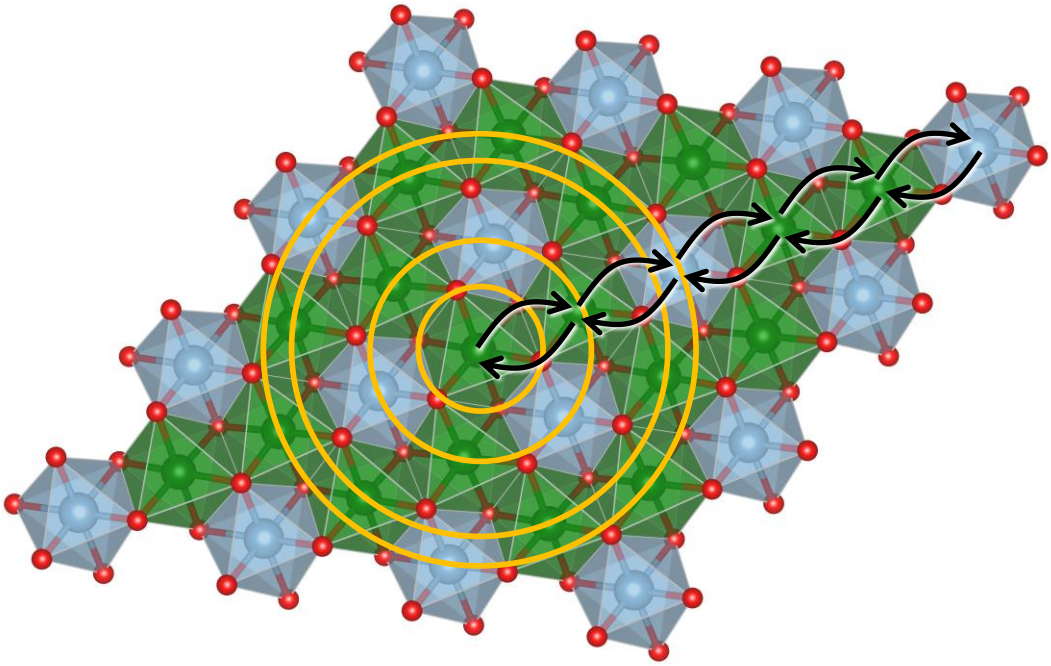

Figure S8 a-c. EXAFS and FT comparison of Ni-Al LDH and α-$Ni(OH)_2$ [using raw data from references 16 and 17]. In **S8a.)** the beat pattern at 8 $Å^{-1}$ is shown along with peak truncation in the LDH spectra between 8-8.5$Å^{-1}$. In **S8b.)** the effect of increasing Al content on the amplitude of the first metal shell in shown, with higher Al content in LDH #2 versus LDH #3. The Ni:Al ratios in LDH #2 and LDH #3 are 1.3 and 4.3, respectively [16]. This increase in Al content decreases the first metal shell amplitude. In **S8c.)** the scattering paths of Ni, Al, and Si in the fit of LDH silicate #1 [17] are shown. These paths illustrate the out-of-phase (destructive) and in-phase (constructive) interference of Al and Si, respectively, with Ni scattering.

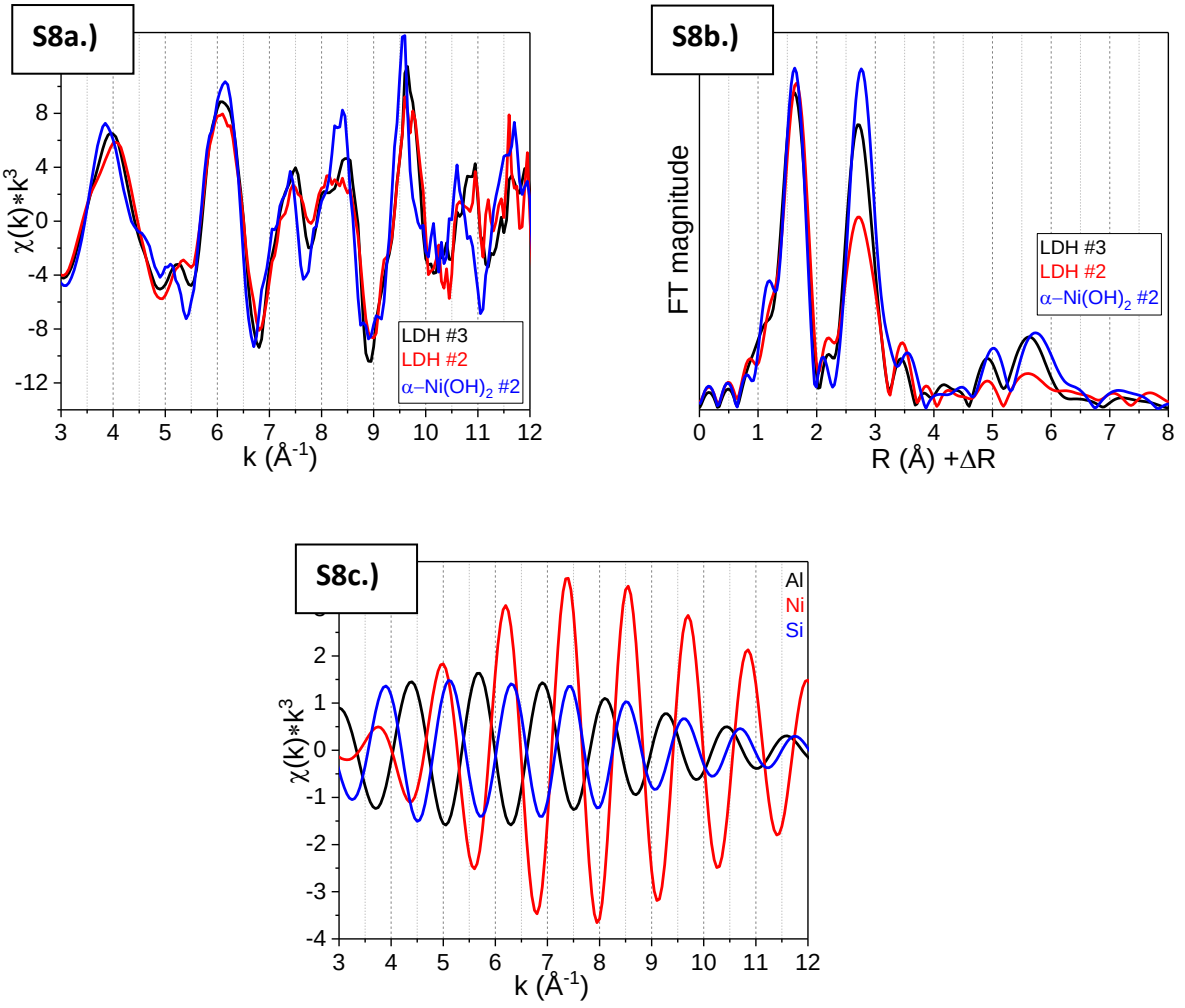

REFERENCES

(1) Ravel, B.; Newville, M. ATHENA, ARTEMIS, HEPHAESTUS: data analysis for X-ray absorption spectroscopy using Ifeffit. *J. Synchrotron Radiat.* **2005,** *12*, 537-541.

(2) Calvin, S. *XAFS for Everyone*; CRC Press: New York, U.S.A., 2013.

(3) Ramesh, T. N.; Kamath, P. V.; Shivakumara, C. Classification of stacking faults and their stepwise elimination during the disorder --> order transformation of nickel hydroxide. *Acta Crystallogr., Sect. B: Struct. Crystallogr. Cryst.Chem.* **2006,** *62*, 530-536.

(4) Mellini, M.; Viti, C. Crystal-structure of lizardite-1t from Elba, Italy. *Am. Mineral.* **1994,** *79*, 1194-1198.

(5) Scheinost, A. C.; Kirsch, R.; Banerjee, D.; Fernandez-Martinez, A.; Zaenker, H.; Funke, H.; Charlet, L. X-ray absorption and photoelectron spectroscopy investigation of selenite reduction by FeII-bearing minerals. *J. Contam. Hydrol.* **2008,** *102*, 228-245.

(6) Funke, H.; Scheinost, A. C.; Chukalina, M. Wavelet analysis of extended X-ray absorption fine structure data. *Phys. Rev. B* **2005,** *71*, 094110.

(7) Funke, H.; Chukalina, M.; Scheinost, A. C. A new FEFF-based wavelet for EXAFS data analysis. *J. Synchrotron Radiat.* **2007,** *14*, 426-432.

(8) Aimoz, L.; Taviot-Gueho, C.; Churakov, S. V.; Chukalina, M.; Dahn, R.; Curti, E.; Bordet, P.; Vespa, M. Anion and cation order in iodide-bearing Mg/Zn-Al layered double hydroxides. *J. Phys. Chem. C* **2012,** *116*, 5460-5475.

(9) Momma, K.; Izumi, F. VESTA 3 for three-dimensional visualization of crystal, volumetric and morphology data. *J. Appl. Crystallogr.* **2011,** *44*, 1272-1276.

(10) Arakcheeva, A. V.; Pushcharovskii, D. Y.; Rastsvetaeva, R. K.; Atensio, D.; Lubman, G. U. Crystal structure of comparative crystal chemistry of $Al_2Mg_4(OH)_{12}(CO_3)\cdot 3H_2O$, a new mineral from the hydrotalcite-manasseite group. *Kristallografiya* **1996,** *41*, 1024-1034.

(11) Balan, E.; Lazzeri, M.; Morin, G.; Mauri, F. First-principles study of the OH-stretching modes of gibbsite. *Am. Mineral.* **2006,** *91*, 115-119.

(12) Mellini, M. The crystal-structure of lizardite 1t - hydrogen-bonds and polytypism. *Am. Mineral.* **1982,** *67*, 587-598.

(13) Gruner, J. W. The crystal structure of kaolinite. *Z.Kristallogr.* **1932,** *83*, 75-88.

(14) Sideris, P. J.; Nielsen, U. G.; Gan, Z. H.; Grey, C. P. Mg/Al ordering in layered double hydroxides revealed by multinuclear NMR spectroscopy. *Science* **2008,** *321*, 113-117.

(15) Cadars, S.; Layrac, G.; Gerardin, C.; Deschamps, M.; Yates, J. R.; Tichit, D.; Massiot, D. Identification and quantification of defects in the cation ordering in Mg/Al layered double hydroxides. *Chem. Mat.* **2011,** *23*, 2821-2831.

(16) Scheinost, A. C.; Sparks, D. L. Formation of layered single- and double-metal hydroxide precipitates at the mineral/water interface: a multiple-scattering XAFS analysis. *J. Colloid Interface Sci.* **2000,** *223*, 167-178.

(17) Peltier, E.; Allada, R.; Navrotsky, A.; Sparks, D. L. Nickel solubility and precipitation in soils: a thermodynamic study. *Clays Clay Miner.* **2006,** *54*, 153-164.